

## Original Article

# Identification of lipid metabolism-related marker genes in colorectal cancer

Bo Gao<sup>1</sup>, Jitao Hu<sup>1</sup>, Hao Wu<sup>2</sup>, Baokun Li<sup>1</sup>

<sup>1</sup>Second Departments Surgery, The Fourth Hospital of Hebei Medical University, Shijiazhuang 050000, Hebei, China; <sup>2</sup>Clinical Laboratory of East Hospital, The Fourth Hospital of Hebei Medical University, Shijiazhuang 050000, Hebei, China

Received December 23, 2024; Accepted April 3, 2025; Epub May 15, 2025; Published May 30, 2025

**Abstract:** Objective: To identify lipid metabolism associated biomarkers in colorectal cancer (CRC). Methods: To refine our list of candidate genes, we utilized the Molecular Complex Detection (MCODE) plug-in within Cytoscape software and performed protein-protein interaction (PPI) network analysis to extract hub genes centrally located within the networks, which potentially possess important regulatory functions. Hub gene-associated miRNAs and transcription factors (TFs) were analyzed using miRNet. Immunohistochemical staining was employed to verify the expression levels of hub genes in clinical CRC tissues. Concurrently, cellular experiments were designed to explore the functional roles of the hub gene DHCR7 at the cellular level, providing scientific evidence for the precision treatment of CRC. Results: A total of 9008 differentially expressed genes (DEGs) were identified between CRC and control samples. Gene Set Enrichment Analysis (GSEA) revealed that these DEGs were mainly enriched in biological processes such as myogenesis, adipogenesis, oxidative phosphorylation, and fatty acid metabolism. Using Weighted Gene Co-expression Network Analysis (WGCNA), we found that the pink and yellow modules were most significantly associated with CRC. Cytoscape analysis identified six hub genes (DHCR7, FABP4, FASN, FAXDC2, PTGIS, SLC27A6). Their diagnostic performance was verified in the external GSE23878 dataset. Clinical studies showed a downregulation trend in the expression of FAXDC2 and PTGIS in CRC tissue samples, while FASN and DHCR7 were up-regulated in colon cancer tissues. However, the expression trend of FABP4 was inconsistent with previous bioinformatics predictions. Further cellular experimental results demonstrated that DHCR7 knockdown significantly inhibited CRC cell proliferation and induced apoptosis, which strongly supported the previous bioinformatics analysis. Conclusion: Our research successfully identified six hub genes in CRC through a series of rigorous analyses and experimental validations. These findings provide important molecular basis for further investigation into the pathogenesis and progression of CRC.

**Keywords:** CRC, hub gene, lipid metabolism-related genes

## Introduction

Cancer incidence and mortality rates have remained high for many years, posing a significant threat to human health. It was predicted that by 2020, approximately 19.3 million new cancer cases would be diagnosed worldwide, while nearly 10 million cancer patients would die from the disease. In China, this situation is particularly severe. Over the past decade, the incidence and mortality rates of colorectal cancer (CRC) have steadily increased, emerging as a prominent health concern [1]. Intermediate and advanced (stage III-IV) CRC accounts for the majority of cancer-related deaths. Although

current treatment strategies, such as surgical resection, systemic chemotherapy, have improved patient outcomes, their efficacy remains limited due to the lack of actionable tumor-specific antigens [2]. Therefore, further exploration of diagnostic biomarkers and therapeutic targets is crucial to develop more precise and effective interventions for CRC patients. Currently, molecular targeted therapy has become a new trend and research direction in the field of CRC treatment due to its high efficiency and low toxicity. Accordingly, studying the molecular mechanisms underlying CRC progression and identifying novel biomarkers for targeted therapy are expected to benefit patient outcome.

## Identifying lipid biomarkers in CRC

Lipid molecules, including fatty acids, glycerides, and other lipids, are fundamental structural components of life. In addition, they play a crucial role as signaling molecules in cellular activities and are involved in energy storage and metabolism [3]. Lipid metabolism is often reprogrammed in tumors, and cancer cells exploit aberrant lipid metabolism to obtain energy, biofilm components, and essential signaling molecules that support their growth [4]. Lipid metabolism is intricately linked to CRC development. Besides the well-known role of lipid-related enzymes in providing energy and building blocks for cancer cells, recent studies have also shown that lipid metabolism-related genes can regulate the tumor microenvironment. For example, lipid-associated signaling pathways can influence the infiltration and function of immune cells in the tumor microenvironment, which in turn affects the immune response against CRC cells. Moreover, abnormal lipid metabolism can lead to the production of bioactive lipid species that modulate cell-cell communication and promote tumor cell invasion and metastasis [5]. Dysregulated lipid metabolism is widely recognized as being closely related to the development of various cancers, including CRC. For example, study has shown that in CRC, the expression of squalene cyclooxygenase, a key rate-limiting enzyme in cholesterol biosynthesis pathway, is significantly upregulated. This upregulation can promote tumor formation through intracellular mechanisms and metabolic regulation of gut microbiota [6]. DAI *et al.* [7] found that PTPRO inhibited CRC development and metastasis by regulating and reprogramming lipid metabolism. The rate-limiting enzyme for fatty acid (FA) synthesis, acetyl coenzyme A carboxylase (ACC), consists of two isoforms (ACC1 and ACC2), and enhanced expression of ACC1 promotes CRC tumor progression and lipid synthesis [8]. Fatty acid synthase (FASN), the main enzyme responsible for fatty acid synthesis, is upregulated in CRC. Study has shown that elevated FASN expression correlates with poor prognosis in CRC and can rescue CRC cells from oxaliplatin-induced apoptosis [9]. Stearoyl coenzyme A desaturase 1 (SCD1) catalyzes the synthesis of unsaturated fatty acids. Literature reports indicate that SCD1 is highly expressed in CRC tissues, and its expression level is negatively correlated with the prognosis of CRC patients. In vitro experiments have further confirmed that SCD1 accel-

erates CRC progression by promoting epithelial-mesenchymal transition (EMT) [10]. The above research emphasizes the crucial role of lipid metabolism-related genes in the pathogenesis and progression of CRC.

Since the turn of the century, gene sequencing technology has evolved rapidly, enabling the identification of molecular prognostic markers for an increasing number of cancers, including CRC. Recent reports suggest that genomic data outperform conventional staging systems in assessing prognostic risk and predicting the benefit of adjuvant chemotherapy. Therefore, screening molecular markers using big data at the transcriptome level holds great promise. In this comprehensive study, we leveraged the resources of the TCGA database to obtain RNA sequencing (RNA-seq) data and detailed clinical information from CRC tumor samples. We then screened lipid metabolism-related genes from a molecular characteristics database and rigorously validated them through a series of experimental methods, aiming to identify key genes closely related to lipid metabolism in CRC.

### Materials and methods

#### *Data source*

We retrieved RNA sequencing (RNA-seq) data and corresponding clinical features for over 600 tumor samples from the Cancer Genome Atlas (TCGA) database, encompassing cases of TCGA-Colon Adenocarcinoma (COAD) and TCGA-Rectum Adenocarcinoma (READ), along with 51 control samples, all sourced from the official website. Additionally, we obtained the GSE23878 dataset from the Gene Expression Omnibus (GEO), which contained 35 CRC samples and 24 control samples. For our research, we designated the TCGA-CRC dataset as the training set and the GSE23878 dataset as the external validation set. On this basis, we meticulously screened out 1,426 genes closely related to lipid metabolism from the Molecular Signatures Database (MSigDB), laying a solid foundation for subsequent analyses.

#### *Screening of DEGs*

In the context of TCGA-CRC, we utilized the DESeq2 package [PMID: 25516281] to identify differentially expressed genes (DEGs) between

## Identifying lipid biomarkers in CRC

CRC and control samples, using the criteria of adj.  $P < 0.05$  and  $|\text{Log}_2 \text{fold change}| > 1$ . Visualization of these DEGs was achieved through heatmaps and volcano plots, generated by R packages such as “pheatmap”. Enrichment pathway analysis was performed using Gene Set Enrichment Analysis (GSEA). The signature gene sets were obtained from MSigDB Collections.

### *Weighted gene co-expression network analysis (WGCNA)*

We adopted the WGCNA R package to construct a gene co-expression network within the TCGA-CRC database. During the initial processing phase, we utilized the ‘hclust’ function to cluster the samples, effectively eliminating outliers and ensuring data quality. Subsequently, using the pick soft-threshold function from the WGCNA package, we carefully selected the optimal soft threshold to ensure the regulatory relationships among genes to conform to the characteristics of a scale-free network distribution. Based on this, we constructed a neighborhood connectivity matrix among gene expression profiles and converted it into a Topological Overlap Matrix (TOM), from which we built a hierarchical clustering tree. Using dynamic pruning methods, we successfully identified multiple gene co-expression modules. Finally, we thoroughly calculated the correlations between these modules and clinical groups, selecting the module with the strongest correlation. The genes within this module were taken as the focus of our subsequent analyses to further explore their potential biological significance.

### *Functional enrichment analysis*

Functional annotation of candidate genes was presented using an R package, including GO (Gene Ontology) and KEGG (Kyoto Encyclopedia of Genes and Genomes) pathway analyses. GO was particularly useful for dissecting the cellular components (CC) and other biological aspects of candidate genes. Statistical significance was considered when the adjusted  $P$ -value was less than 0.05.

### *Construction of PPI network and identification of hub genes*

The PPI (Protein-Protein Interaction) network was constructed using the STRING (Search Tool

for the Retrieval of Interacting Genes/Proteins) database. Afterward, we employed software and its plugin to screen for hub genes. The “GOSemSim” package was used to calculate the semantic similarity of gene classes. The Corrplot software package was used to analyze the correlation between hub genes. To further investigate the potential role of hub genes in immunotherapy, we adopted the Tumor Immune Dysfunction and Exclusion (TIDE) algorithm to assess the immunotherapy sensitivity of CRC patients.

### *Construction of hub genes-miRNA regulatory network*

In this study, we leveraged the miRNet database to accurately predict the potential roles of upstream transcription factors (TFs) and microRNAs (miRNAs). To visually represent these complex interactions, we used Cytoscape software to construct a detailed miRNA/TF-hub gene network diagram. In this network, blue nodes represent the crucial hub genes that play a central role in the entire regulatory network; purple nodes symbolize TFs, which influence various cellular functions by regulating gene expression; and orange nodes stand for miRNAs, small RNA molecules that regulate gene expression at the post-transcriptional level.

### *ROC curve analysis*

ROC (Receiver Operating Characteristic) analysis was conducted using the “pROC” package in R. The primary purpose of this analysis was to evaluate the diagnostic value of central genes for CRC. Specifically, a central gene was considered to have practical diagnostic value for the disease if its AUC (Area Under the Curve) value exceeded 0.7, indicating a high ability to distinguish CRC patients from healthy individuals.

### *Clinical information*

From January 2019 to January 2022, the General Surgery Department of the Fourth Hospital of Hebei Medical University admitted and treated a total of 54 CRC patients. Among these, 31 were male and 23 were female. The youngest patient was 26 years old, and the oldest was 79 years old, with an average age of 64.31 years (standard deviation = 9.29). Tumor location: 29 cases of rectum and 25 cases of

## Identifying lipid biomarkers in CRC

colon. Lymph node metastasis was observed in 18 cases. Tumor diameters were  $\leq 5$  cm in 40 cases and  $> 5$  cm in 14 cases. Regarding TNM stage, 37 cases were classified as stage I-II, and 17 cases were classified as stage III. Tumor differentiation was high or moderate in 35 cases, and low in 19 cases. The study was approved by the ethics committee of the Fourth Hospital of Hebei Medical University, and all patients provided informed consent. Inclusion criteria: diagnosis of CRC confirmed by postoperative pathological examination; all patients were primary cases; complete clinical data. Exclusion criteria: age  $< 18$  years or  $> 80$  years; preoperative neoadjuvant radiotherapy or targeted therapy; recurrent CRC, hereditary CRC, or combination of other malignant tumors; serious organ failure; pneumonia, urinary tract infection, or other infectious diseases.

### *Immunohistochemical staining*

During surgery, portions of CRC tumor tissue and adjacent tissue (more than 5 cm from the tumor edge) were obtained, with each sample carefully preserved at approximately 100 milligrams. The CRC tumor and adjacent tissues were then placed in a standard 10% formalin solution for 12 hours of fixation. After fixation, the tissues were embedded in paraffin and sectioned. The primary antibody was added to the sections and incubated at 4°C overnight. The following day, HRP-conjugated sheep anti-rabbit secondary antibody was added and incubated at 37°C for 60 mins. DAB color development was performed for 5 min, followed by re-staining with hematoxylin. Hydrochloric acid alcohol was used for differentiation, gradient ethanol was used for dehydration. Finally, the samples were sealed with neutral gum and observed under a microscope.

### *Cell culture and transfection procedures*

DEME medium was used to culture the SW620 and HT-29 cell lines, supplemented with 10% fetal bovine serum, 100 U/ml penicillin, and 100  $\mu\text{g}/\text{ml}$  streptomycin to ensure optimal cell growth. The cells were cultivated in a standard incubator at 37°C with 5%  $\text{CO}_2$ . When cell confluence reached approximately 80%, 0.25% trypsin-EDTA was used for cell passage. For transfection, cells in the logarithmic growth phase were selected and seeded into 6-well plates at a density of  $5 \times 10^5$  cells per well. Then,

DHCR7 shRNA and negative control (NC) shRNA were transfected into the cells, following the Lipofectamine 3000 reagent protocol, with three wells set up for each condition to ensure experimental accuracy. After a transfection period of 48-72 hours, relevant assays were conducted to assess gene function and elucidate the underlying mechanisms.

### *Clonogenic cell assay*

Cells in the logarithmic growth phase were harvested using trypsinization to prepare a single-cell suspension, which was then evenly dispensed onto 6-well plates at a density of approximately 500 cells per well, with three replicate wells for each condition. Subsequently, the cells were placed in DMEM medium containing 10% fetal bovine serum and incubated in a constant-temperature incubator for 10 to 14 days. After incubation, the medium was carefully removed, and the cells were washed with PBS. The cells were then fixed with 4% paraformaldehyde for 15 minutes and stained with 0.1% crystal violet for 10 minutes. To remove excess stain, the 6-well plates were rinsed with running buffer and air-dried. Finally, the plates were observed and counted under a microscope to assess changes in cell proliferation and analyze the impact of the target gene on CRC cell proliferation.

### *Wound healing assay*

The cells were evenly plated in a 6-well plate and cultured under appropriate conditions until they reached approximately 90% confluence, forming a dense monolayer. Next, a sterile 200 $\mu\text{l}$  pipette tip was used to make a precise and uniform scratch on the monolayer, creating a clear wound area. The plate was subsequently rinsed multiple times with PBS solution to remove any cells that detached during the scratching. Serum-free medium was added, and the plate was placed in an incubator for continued culture. At regular intervals, the wound closure was observed under a microscope, and images were captured for documentation. Finally, the width of the scratch was precisely measured using ImageJ software, and the cell migration rate was calculated:  $\text{Migration rate} = (\text{Initial scratch width} - \text{Scratch width at each time point}) / \text{Initial scratch width} \times 100\%$ . This calculation allowed us to assess the

## Identifying lipid biomarkers in CRC

changes in cellular migratory capacity following modulation of the target gene.

### *Transwell invasion assay*

Prior to the experiment, 8  $\mu\text{m}$ -pore Transwell inserts were pre-coated with 50  $\mu\text{L}$  of Matrigel matrix (thawed at 4°C) and incubated at 37°C for 4-6 hours to solidify. Cells at logarithmic phase were trypsinized, resuspended in serum-free medium at  $5 \times 10^5$  cells/mL, and 100  $\mu\text{L}$  aliquots were seeded into the upper chambers while 600  $\mu\text{L}$  of 10% FBS medium served as chemoattractant in the lower chambers. After 24-hour incubation (37°C, 5%  $\text{CO}_2$ ), non-invaded cells were removed by PBS washing and cotton swab abrasion, while invaded cells on the membrane's lower surface were fixed with 4% paraformaldehyde (20 min), stained with 0.1% crystal violet (15 min), and quantified by counting five random microscopic fields per insert to determine invasive potential.

### *TUNEL assay for apoptosis detection*

After transfection, the cells were evenly plated onto a 6-well plate pre-placed with cover glasses and further cultured until the desired cell density was reached. Subsequently, the original growth medium was aspirated, and the cells were rinsed with PBS. The cells were fixed with 4% paraformaldehyde for half an hour. After fixation, the cells were rinsed again with PBS and permeabilized with Triton X-100 for 15 minutes. Following permeabilization, the cells were rinsed once more with PBS. Next, the TUNEL assay was performed according to the manufacturer's instructions: the TUNEL reaction mixture was added to the cells and incubated in a dark, humidified chamber at 37°C for 1 hour. After incubation, the cells were thoroughly washed with PBS and stained with DAPI to highlight the nuclei. After another wash with PBS, the samples were examined under a fluorescence microscope, where green fluorescence (indicating apoptotic cells) and blue fluorescence (representing cell nuclei) were observed using excitation wavelengths of 450-500 nm. Apoptotic cells were counted in randomly selected areas, and the apoptosis rate was calculated as the percentage of apoptotic cells to the total cell count, to assess the impact of the target gene on cellular apoptosis.

### *Reverse transcription quantitative PCR (RT-qPCR)*

Following the provided protocol, cells in their logarithmic growth phase were collected, and total RNA was isolated using TRIzol reagent. Subsequently, the purity and concentration of the RNA were assessed with a spectrophotometer, revealing an A260/A280 ratio between 1.8 and 2.0. Using a reverse transcription kit, 1  $\mu\text{g}$  of total RNA was reverse transcribed into complementary DNA (cDNA) under the following conditions: 5 minutes at 25°C, 30 minutes at 42°C, and a final 5-minute treatment at 85°C. Quantitative PCR was performed in a 20  $\mu\text{L}$  reaction volume using cDNA as the template. The qPCR program included an initial denaturation at 95°C for 10 minutes, followed by 40 cycles of amplification at 95°C for 15 seconds and 60°C for 1 minute, concluding with a melting curve analysis to confirm amplification specificity. To ensure reproducibility, three independent experiments were conducted, and the relative expression level of the target gene was determined using the  $2^{-\Delta\Delta\text{Ct}}$  method, with GAPDH serving as the endogenous control. The experiments were repeated three times to ensure accuracy, allowing precise measurement of gene expression changes.

### *Western blot analysis*

After a series of treatments, the cells were collected, and total protein was extracted through a lysis process. Subsequently, the protein concentration was quantified using a BCA protein assay kit. Equal amounts of protein samples were mixed with loading buffer and subjected to heat denaturation at boiling temperature for 5 minutes. Following this, the proteins were effectively separated by SDS-PAGE electrophoresis, with the stacking gel voltage set at 80 V and the resolving gel voltage at 120 V. Upon completion of electrophoresis, the proteins were transferred to a PVDF membrane at a constant current of 300 mA for 90 minutes. At room temperature, the PVDF membrane was blocked for 60 minutes using 5% skimmed milk. The membrane was then incubated overnight at 4°C with a DHCR7-specific primary antibody and a  $\beta$ -actin antibody as a loading control. After washing, the membrane was incubated with a secondary antibody at room temperature for 1 hour and washed again three times

## Identifying lipid biomarkers in CRC

with TBST. The protein bands were observed using ECL chemiluminescent solution, and their intensities were quantified using ImageJ software.

### *Statistical analysis*

Statistical analyses were performed using R and SPSS software. Continuous data were expressed as mean  $\pm$  standard deviation ( $x \pm s$ ). For comparisons between two groups, an independent sample t-test was used; for comparisons among multiple groups, one-way ANOVA was applied, with Tukey's post-hoc test for pair-wise comparisons. Categorical data were expressed as counts and percentages, and differences between groups were assessed using the chi-square test or Fisher's exact test (for smaller sample sizes). To generate the Receiver Operating Characteristic (ROC) curve, the "pROC" package was used to calculate the Area Under the Curve (AUC), which served as a key indicator of diagnostic performance. An AUC value exceeding 0.7 was considered indicative of a significant difference. The significance level was set at 0.05, and a *P*-value less than 0.05 was considered statistically significant. This meticulous approach to data analysis ensured accurate interpretation of the experimental results, revealing the intrinsic significance of the data and providing a solid statistical foundation for the study's conclusions.

## Results

### *DEGs in CRC and control*

This study successfully collected RNA-seq data and clinical characteristics from over 600 tumor samples, including cases of TCGA-colon adenocarcinoma and TCGA-rectal adenocarcinoma, along with 51 normal control samples. Using these datasets, this study screened a total of 9008 DEGs, with more than 5000 upregulated genes and over 3000 downregulated genes (**Figure 1A**). As shown in **Figure 1B**, in addition to the overall analysis of DEGs, we specifically focused on lipid metabolism-related genes, including RETSAT, SLC51A, SLC22A5, PEX26, PHLPP2, CIPC, ETFDH, APPL2, UGP2, PDCD4, CLEC3B, GLTP, TEX11, BEST4, SLC25A34, GRIN2D, PDX1, CPNE7, SIM2, FOXQ1, CEMIP, MTHFD1L, TRIB3, AJUBA, CLDN1, and CST1. Among these, RETSAT, which is involved in retinol metabolism, was downreg-

ulated in CRC samples compared to controls. SLC51A, which is related to lipid transport, showed upregulated expression. These differential expression patterns suggest potential disruptions in lipid-related processes, like retinol-based signaling and lipid transportation, in CRC. Furthermore, analysis indicated that these DEGs were primarily enriched in biological processes such as myogenesis and adipogenesis (**Figure 1C**).

### *Construction of co-expression networks*

Based on the sample clustering tree, we identified four significant abnormal samples, which are clearly presented in **Figure 2A, 2B**. After precise calculations, the optimal soft threshold power was determined to be 7, as intuitively displayed in **Figure 2C**. In the co-expression network, we successfully identified 14 key modules, as detailed in **Figure 2D**. Furthermore, the results of the module-trait relationships revealed the highest correlation between the pink and yellow modules and CRC, as shown in **Figure 2E**. Thus, 1640 genes in the pink and yellow modules were selected for further investigation.

### *Functional enrichment analysis*

An in-depth analysis was conducted on the gene intersections within the aforementioned modules, specifically focusing on the intersection of DEGs, lipid metabolism-related genes, and specific genes. Using a Venn diagram for visualization, we identified 41 candidate genes in this intersection, as shown in **Figure 3A**. Subsequently, GO analysis of these candidate genes revealed that they were primarily enriched in processes such as lipid metabolism and fatty acid metabolism, as shown in **Figure 3B**. In addition, KEGG enrichment analysis also indicated that these candidate genes were significantly involved in processes such as the Ras signaling pathway, as shown in **Figure 3C**.

### *PPI network and hub gene identification*

We utilized the STRING database to construct a PPI network encompassing 41 candidate genes, as illustrated in **Figure 4A**. With the assistance of the MCODE plugin, we successfully identified six hub genes, as shown in **Figure 4B**. Functional similarity analysis revealed that FAXDC2 scored the highest, as depicted in

# Identifying lipid biomarkers in CRC

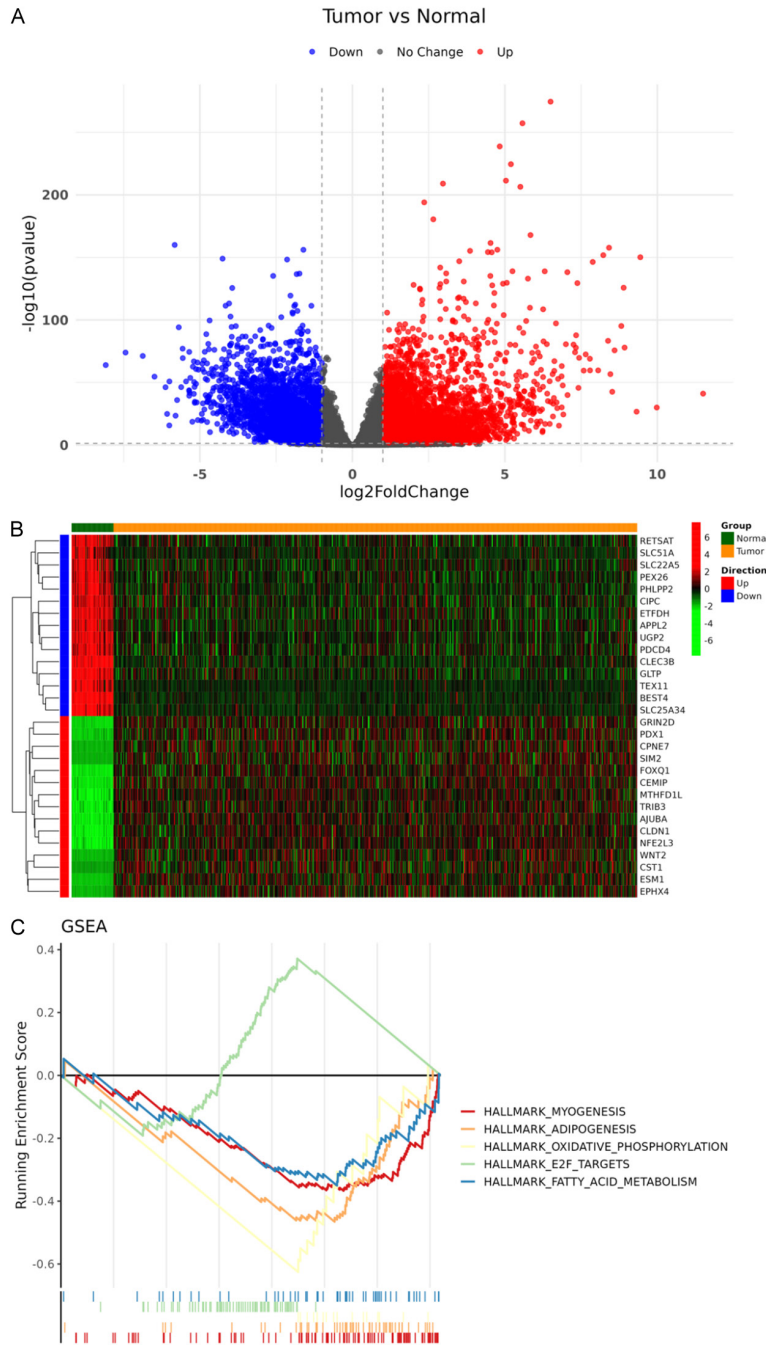


**Figure 1.** DEGs in CRC and control. A: The volcano plot displays differentially expressed genes (DEGs) between CRC samples and control samples in The Cancer Genome Atlas - Colorectal Cancer (TCGA-CRC) database, where red represents upregulated DEGs and blue represents downregulated DEGs. B: The heatmap visually presents the DEGs between CRC samples and control samples in the TCGA-CRC database. C: The enrichment pathway analysis of DEGs was performed using Gene Set Enrichment Analysis (GSEA).

**Figure 4C.** In addition, a strong correlation was found between FASN and DHCR7 ( $r = 0.73$ , **Figure 4D**). The correlation between hub gene

expression and TIDE score showed that DHCR7 gene was associated with immune exclusion, while the remaining five genes were associated with immune disorders (**Figure 4E**).

## Prediction of potential miRNA/TF-hub gene regulatory network

We constructed a miRNA/TF-hub gene regulatory network diagram for the previously identified key genes, as shown in **Figure 5**. To better understand the transcriptional regulatory mechanisms involving these hub genes, we utilized Cytoscape software to construct the miRNA-hub gene TF regulatory network. The analysis revealed that FASN was the hub gene regulated by most miRNAs, while FABP4 was the hub gene regulated by most TFs.

## The ROC curve analysis and expression analysis of hub genes

To investigate the expression of these genes in CRC, we extracted and compared the expression data of hub genes between CRC patients and normal controls from the TCGA database (**Figure 6A**). The results showed that the expression levels of FABP4, FAXDC2, PTGIS, and SLC27A6 were downregulated in CRC patients, while the expression levels of DHCR7 and FASN were upregulated. Next, we evaluated the diagnostic value of these genes in CRC by analyzing ROC curves. As shown in **Figure 6B**, the ROC

curves of the six hub genes clearly demonstrated their diagnostic performance. Specifically, the AUC values for DHCR7, FABP4, FASN,

## Identifying lipid biomarkers in CRC

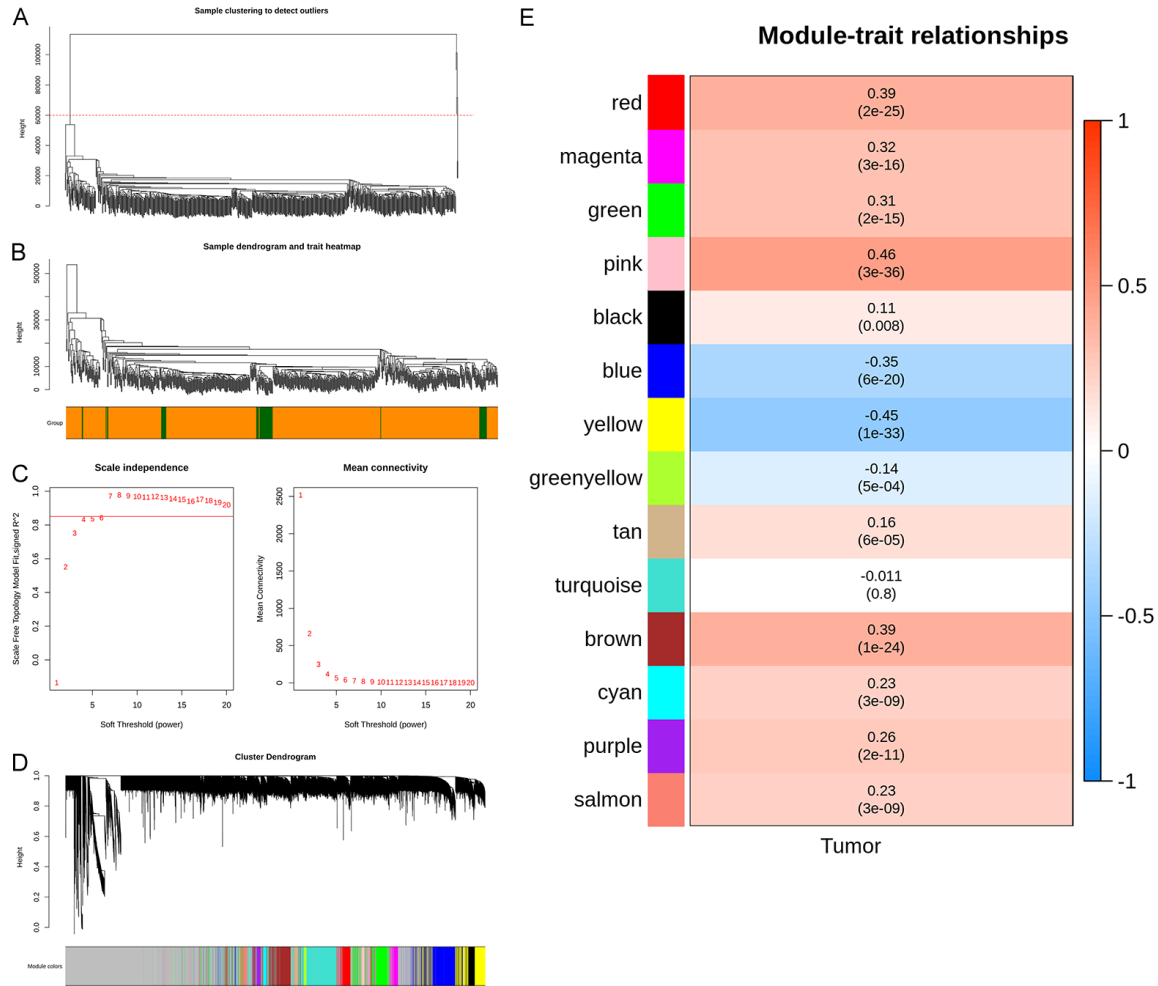


**Figure 2.** Construction of a shared expression network. A, B: The sample clustering diagram reveals the presence of outliers. C: To construct a standard scale-free network, we have determined an appropriate soft threshold power  $\beta$ . D: Association between each module and colorectal cancer (CRC) was analyzed by calculating gene significance (GS) and module membership degree (MM). E: The heatmap illustrates the correlation between gene co-expression modules and CRC. Each row represents a module, and each column represents the tumor trait. The number in each cell indicates the correlation coefficient (upper value) and corresponding  $p$ -value (lower value in parentheses).

FAXDC2, PTGIS, and SLC27A6 were 0.911, 0.933, 0.894, 0.884, 0.833, and 0.972, respectively, indicating that these six hub genes all have good application value in CRC diagnosis.

### Validation of hub genes in GSE23878

We further validated the expression of the six hub genes in CRC tissues using the GSE23878 dataset. As shown in **Figure 7A**, the expression of FABP4, FAXDC2, and PTGIS showed a down-regulation trend in CRC tissues, while the expression of DHCR7 and FASN was significantly upregulated. Notably, except for SLC27A6, which had an AUC of 0.673, the AUCs for all other genes were greater than 0.7 (**Figure 7B**).

### Validation of the expression of 6 hub genes in clinical CRC tissues

In this study, we collected 54 pairs of CRC tissues and corresponding adjacent non-cancerous tissue samples and systematically verified the expression levels of the six hub genes using immunohistochemical staining techniques. The results confirmed that, as predicted by bioinformatics, the expression of FAXDC2 and PTGIS was downregulated in CRC tissues, and FASN and DHCR7 were upregulated. However, the expression trends of FABP4 and SLC27A6 were inconsistent with previous bioinformatics predictions. Specifically, FABP4 expression significantly increased in CRC tissues, while no significant difference in SLC27A6 expression was

## Identifying lipid biomarkers in CRC

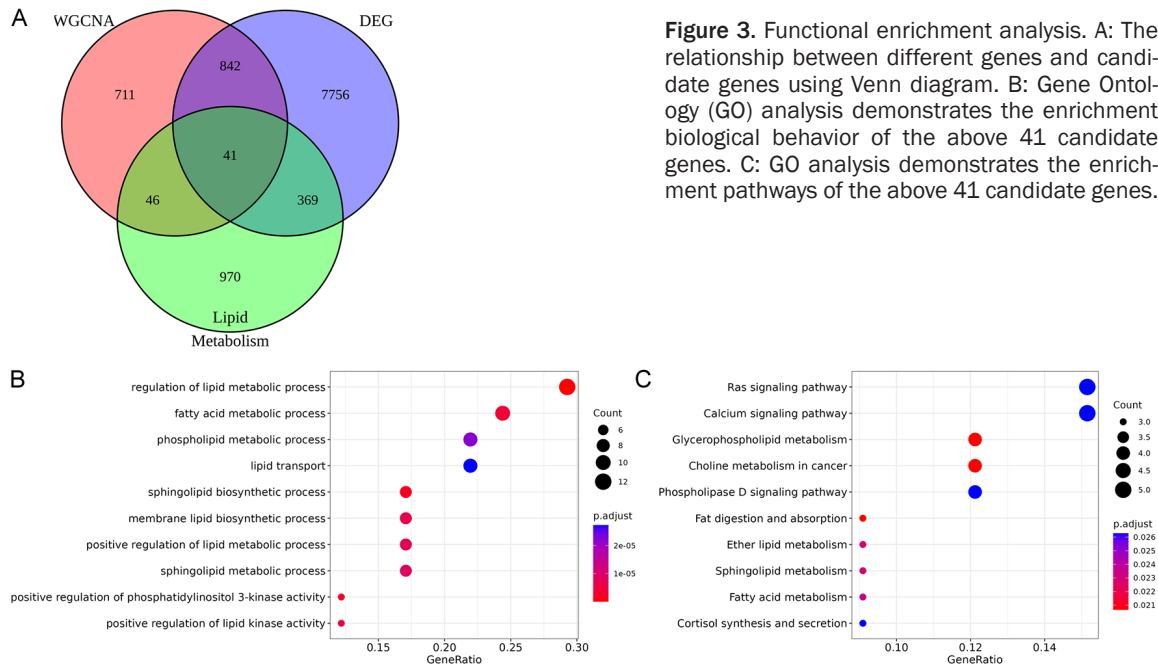


**Figure 3.** Functional enrichment analysis. A: The relationship between different genes and candidate genes using Venn diagram. B: Gene Ontology (GO) analysis demonstrates the enrichment biological behavior of the above 41 candidate genes. C: GO analysis demonstrates the enrichment pathways of the above 41 candidate genes.

observed between CRC tissues and adjacent non-cancerous tissues, deviating from the expected results (**Figure 8**).

*DHCR7 functions as an oncogene to enhance CRC cell proliferation, migration, and invasion*

To substantiate the bioinformatics findings, we focused on DHCR7, a gene that is upregulated in CRC, for further investigation. We transfected CRC cell lines SW620 and HT-29 with DHCR7 shRNA#1, DHCR7 shRNA#2, and DHCR7 shRNA#3 to suppress DHCR7 expression. Among these, DHCR7 shRNA#2 demonstrated the highest effectiveness in reducing both DHCR7 mRNA and protein levels (**Figure 9A, 9B**), and was selected for further studies. Subsequent colony formation experiments revealed the impact of DHCR7 on CRC cell proliferation. The results indicated that DHCR7 knockdown significantly decreased the number of colonies formed by SW620 and HT-29 cells, demonstrating inhibition of cell proliferation, as shown in **Figure 9C**. Additionally, cell scratch assay and Transwell invasion assay showed that DHCR7 knockdown reduced the migration and invasion abilities of SW620 and HT-29 cells, further confirming the crucial role of DHCR7 in CRC cell growth and metastasis (**Figure 9D, 9E**). Collectively, these findings indicate that DHCR7 knockdown significantly impedes the proliferative, migratory, and inva-

sive properties of CRC cells, thereby validating the bioinformatics outcomes for DHCR7.

*Depletion of DHCR7 induced apoptosis in CRC cells*

To further explore the functional role of DHCR7 in CRC, we designed and conducted a series of experiments to assess the specific impact of DHCR7 knockout on apoptosis of CRC cell lines SW620 and HT-29. The TUNEL assay, a sensitive and widely recognized method for detecting DNA fragmentation, was employed to detect apoptotic cell death. The results demonstrated a notable increase in green fluorescence intensity, indicative of TUNEL-positive cells, following the knockdown of DHCR7 in both SW620 and HT-29 cells (**Figure 10**). This increase in fluorescence intensity reflects the elevated number of apoptotic cells, suggesting that DHCR7 depletion triggers apoptosis in CRC cells.

These findings not only validate the bioinformatics prediction that DHCR7 may function as an oncogene in CRC but also underscore the therapeutic potential of targeting DHCR7 to induce apoptosis in cancer cells. By implementing DHCR7 knockout technology to induce programmed cell death (apoptosis), we open a promising avenue for developing novel therapeutic strategies to combat CRC.

# Identifying lipid biomarkers in CRC

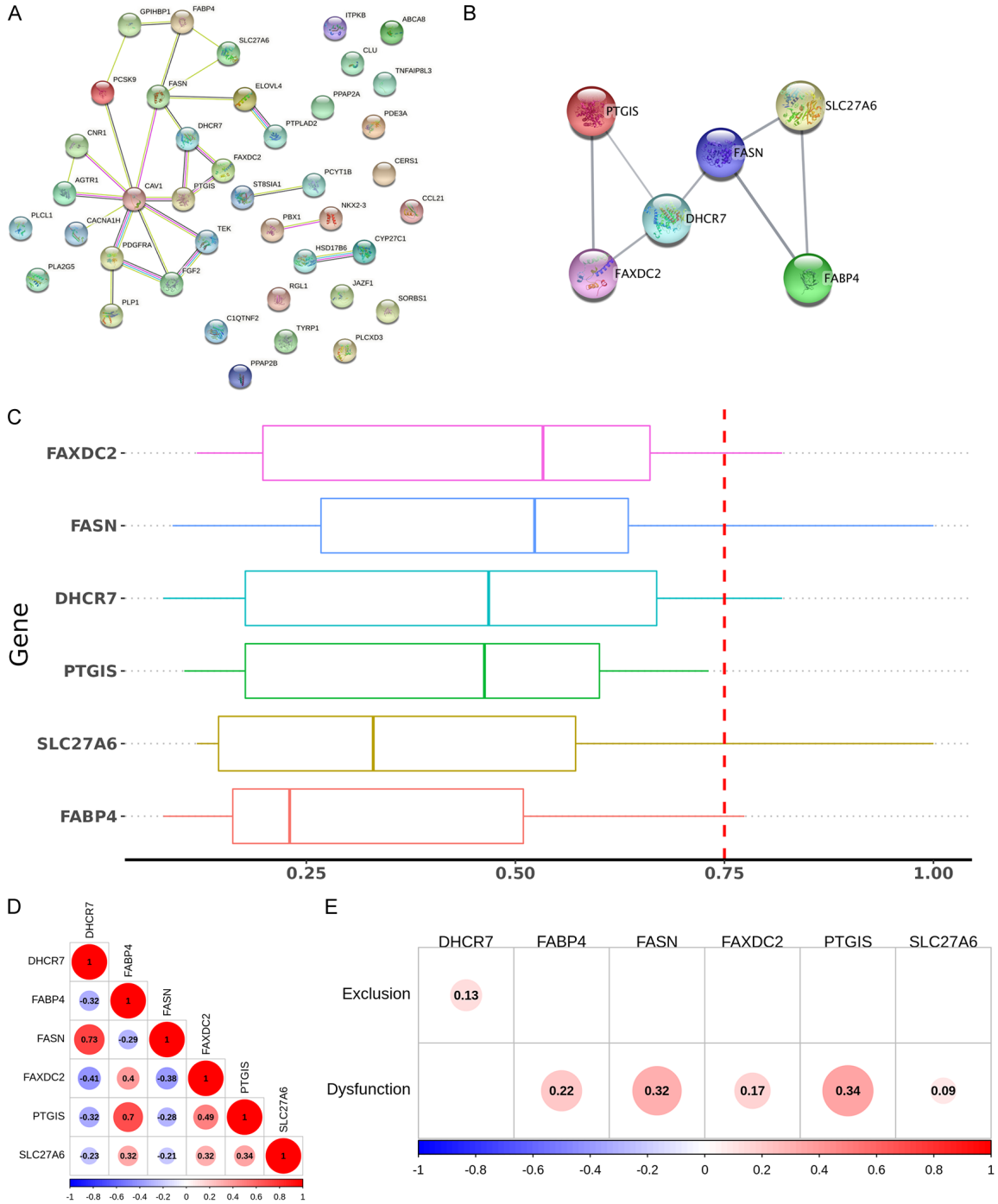


**Figure 4.** Protein-protein interaction network and identification of central genes. A: Protein-Protein Interaction (PPI) network analysis of 41 candidate genes (Known interactions: Blue and purple lines; Predicted interactions: Green, dark blue and red lines; Others: Light green, black and light blue lines). B: Key genes are displayed, including DHCR7, FABP4, FASN, FAXDC2, PTGIS, SLC27A6. C: Functional similarity analysis of the six key genes. D: Correlation analysis of key genes. E: Correlating key genes with Tumor Immune Dysfunction and Exclusion (TIDE) score.

## Discussion

To achieve a balance between precision and comprehensiveness in diagnosis and treat-

ment of CRC, this study adopted a relatively novel approach by screening genes, including hub genes identified through overlapping WGCNA module genes, DEGs and lipid metabo-

## Identifying lipid biomarkers in CRC

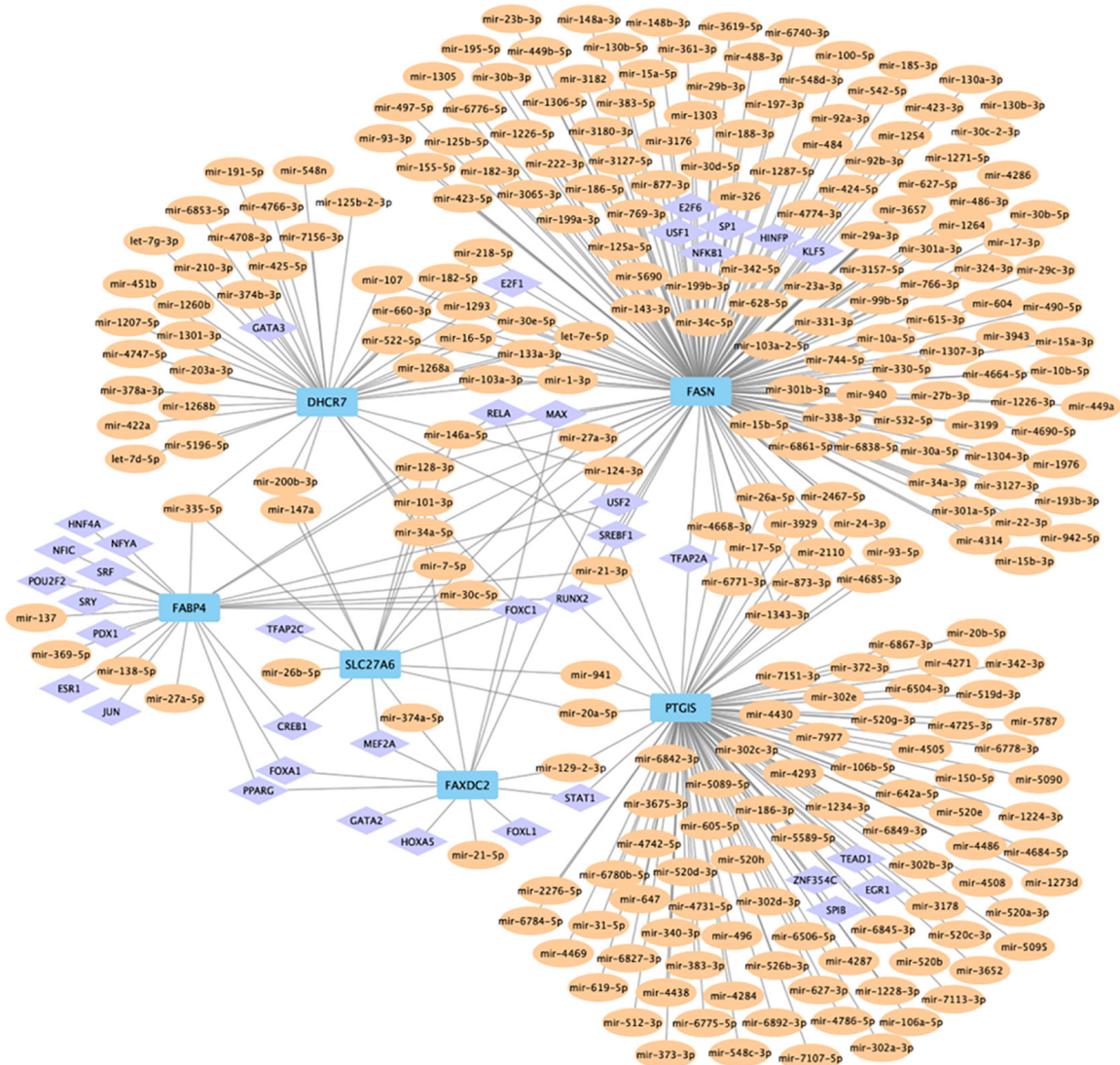


**Figure 5.** Predicting potential miRNA/TF hub gene regulatory networks. miRNAs are represented by orange nodes, TFs by purple nodes, and hub genes by blue nodes.

lism-related genes, followed by gene action pathway analysis. Through rigorous validation using ROC curve analysis, external datasets, and clinical tissue specimen comparisons, we identified six lipid metabolism-related genes (DHCR7, FABP4, FASN, FAXDC2, PTGIS, and SLC27A6) demonstrating strong associations with colorectal cancer pathogenesis. These molecular targets may hold promise for future diagnostic and therapeutic applications.

Enrichment analysis of these DEGs showed that they were mainly enriched in pathways related to fatty acid metabolism, which led us to focus on biomarkers associated with lipid

metabolism. To gain a deeper understanding of the interactions between these genes, WGCNA was employed to construct a gene co-expression network closely related to CRC. Among the 14 gene modules identified by the WGCNA method, the pink and yellow modules were most strongly correlated with CRC, and were therefore selected for further detailed analysis. After screening, this study ultimately identified lipid metabolism-related DEGs [11]. As early as the 1920s, Warburg found that tumor tissues, unlike normal tissues that convert glucose to lactate only under hypoxic conditions, convert glucose to lactate even under well-oxygenated conditions. This process generates adenosine

## Identifying lipid biomarkers in CRC

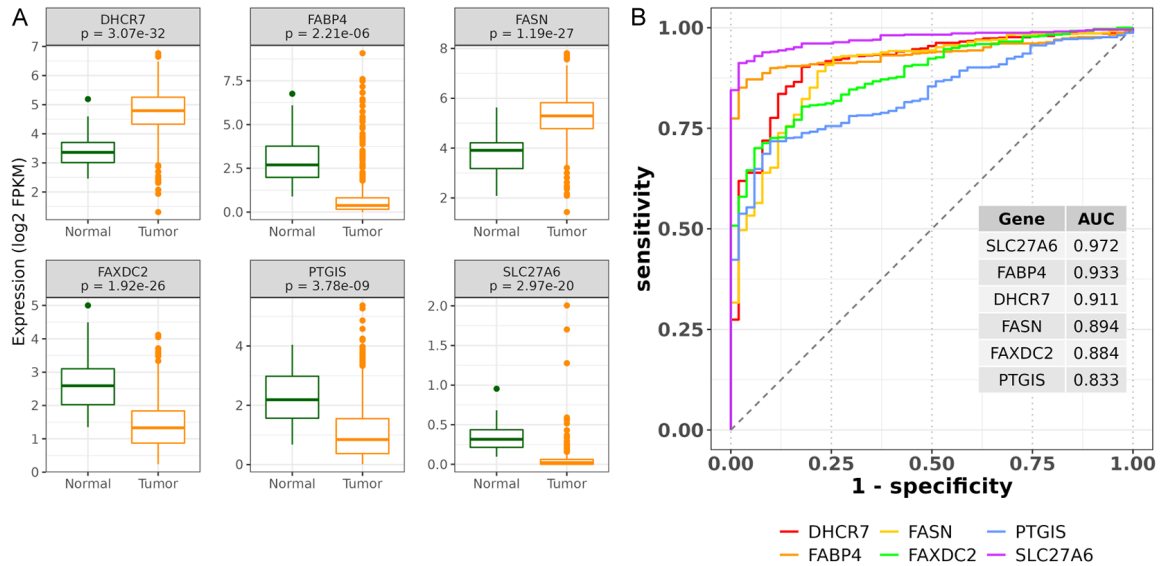


**Figure 6.** Expression of hub genes and their diagnostic value. A: Expression of DHCR7, FABP4, FASN, FAXDC2, PTGIS, and SLC27A6 in The Cancer Genome Atlas - Colorectal Cancer (TCGA-CRC). B: Receiver Operating Characteristic (ROC) curves demonstrates the diagnostic value of 6 hub genes in TCGA-CRC.

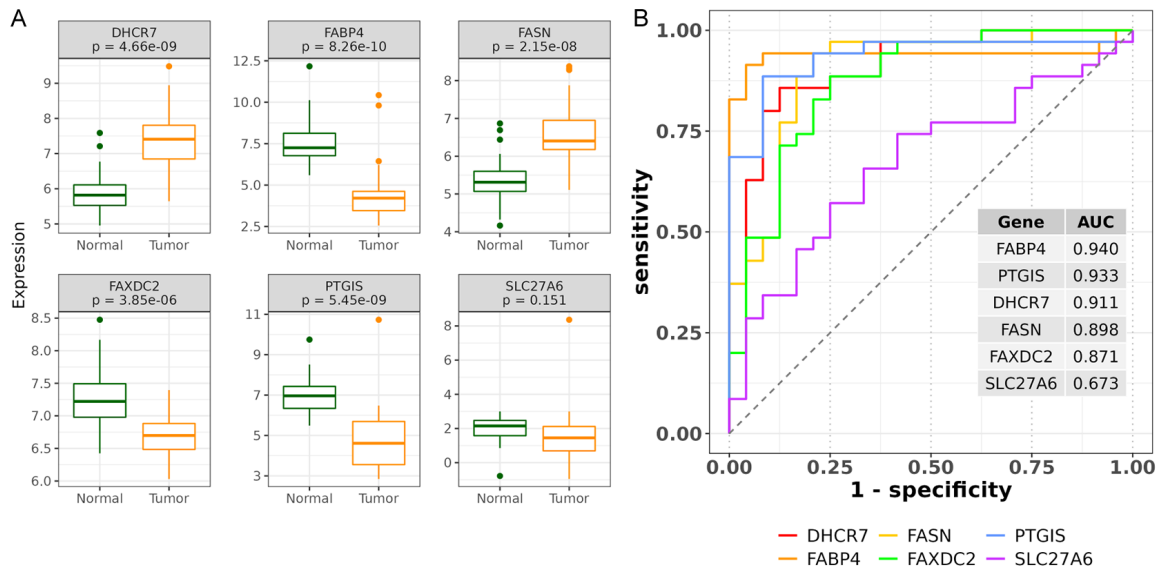


**Figure 7.** Validation of hub genes in GSE23878 dataset. A: Expression of DHCR7, FABP4, FASN, FAXDC2, PTGIS, and SLC27A6 in GSE23878 dataset. B: The Receiver Operating Characteristic (ROC) curve demonstrates the diagnostic efficacy of central genes in the dataset.

triphosphate (ATP) through aerobic glycolysis rather than mitochondrial oxidation [12]. This 'change', known as the 'Warburg effect', marked the beginning of a new era in metabolic reprogramming in tumors. This metabolic shift provides abundant ATP and nutrients, supporting the rapid and uncontrolled proliferation of tumor cells. Lipids play a crucial role in the

development of tumors, not only contributing to the formation and stability of tumor cell membranes but also providing necessary energy for cell growth and division. Additionally, lipids are involved in generating signaling molecules that regulate tumor cell behavior [13]. Therefore, fatty acid oxidation, uptake, and lipogenesis are upregulated in tumor cells. Recent studies

## Identifying lipid biomarkers in CRC

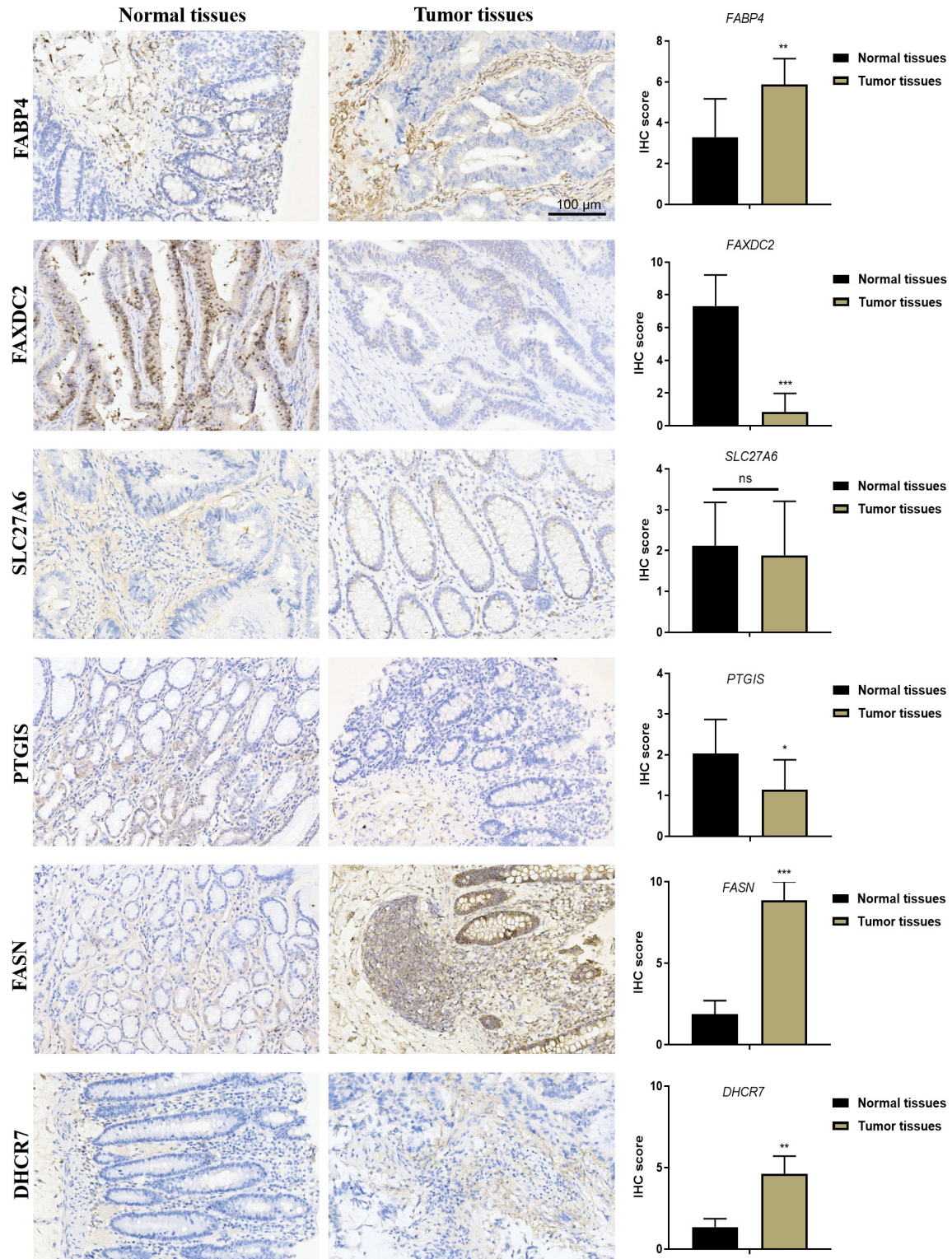


**Figure 8.** Expression of different hub genes in clinical CRC tissues. Immunohistochemical staining was used to examine the expression levels of six hub genes in Colorectal Cancer (CRC) tissues and adjacent tissues. Scale bar: 100  $\mu$ m, 100 $\times$ . Data: Mean  $\pm$  Standard Error of the Mean (SEM), n = 54. \*P < 0.05, \*\*P < 0.01, \*\*\*P < 0.001, compared to normal tissues.

# Identifying lipid biomarkers in CRC

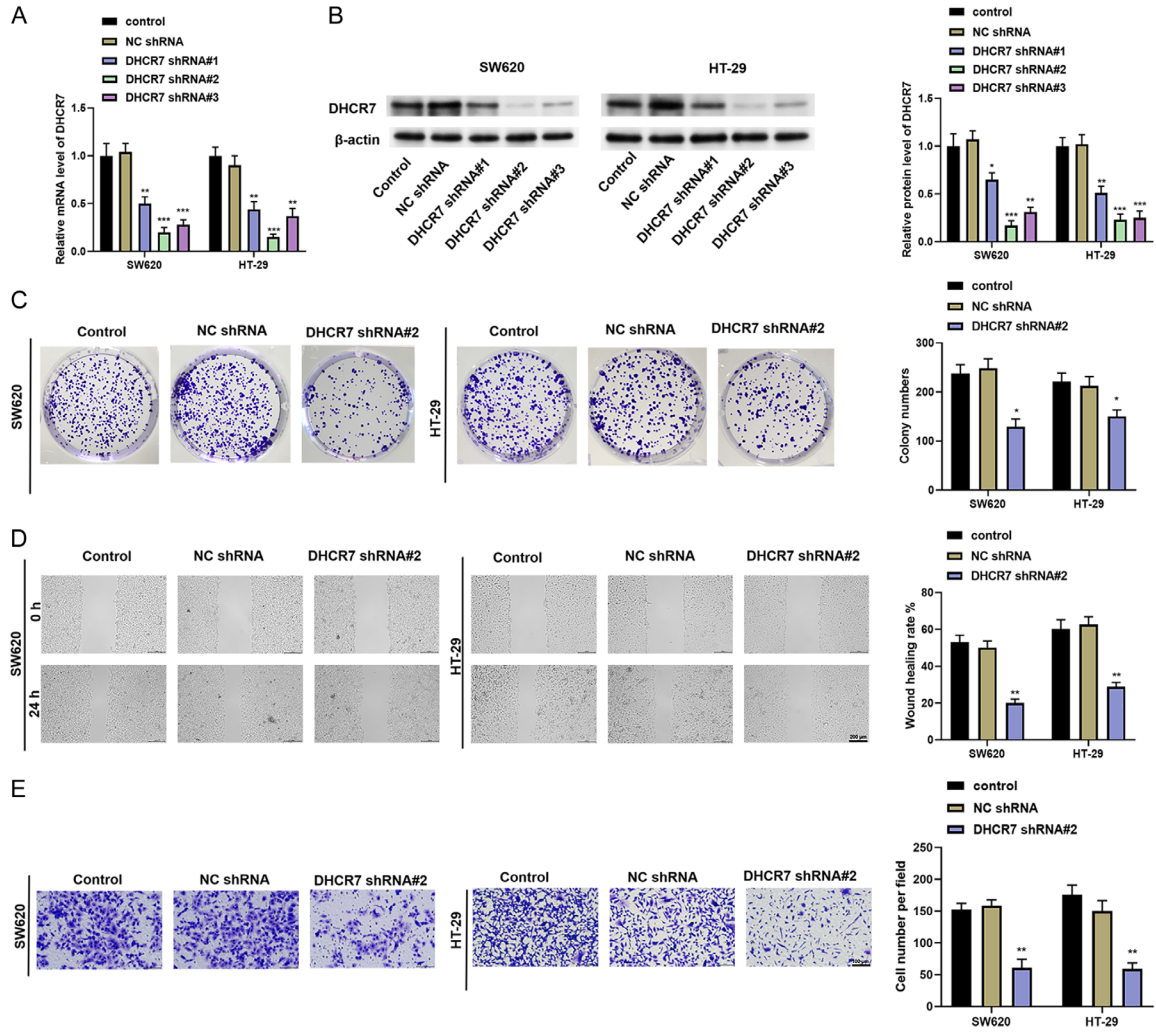


**Figure 9.** DHCR7 functions as an oncogene to enhance CRC cell proliferation, migration, and invasion. A: The mRNA expression of DHCR7 in cells transfected with DHCR7 shRNAs. B: The protein expression of DHCR7 in cells transfected with DHCR7 shRNAs. C: The proliferation of CRC cells after transfection with DHCR7 shRNA # 2 detected by clone formation assay. D: The migration of CRC cells after transfection with DHCR7 shRNA # 2 detected using wound healing assay. Scale bar: 200  $\mu$ m, 50 $\times$ . E: The invasion potential of different CRC cells after transfection with DHCR7 shRNA # 2 examined using Transwell invasion assay. Scale bar: 100  $\mu$ m, 100 $\times$ . Data: Mean  $\pm$  Standard Error of the Mean (SEM), n = 3. \*P < 0.05, \*\*P < 0.01, \*\*\*P < 0.001, compared to Negative Control (NC) shRNA group.

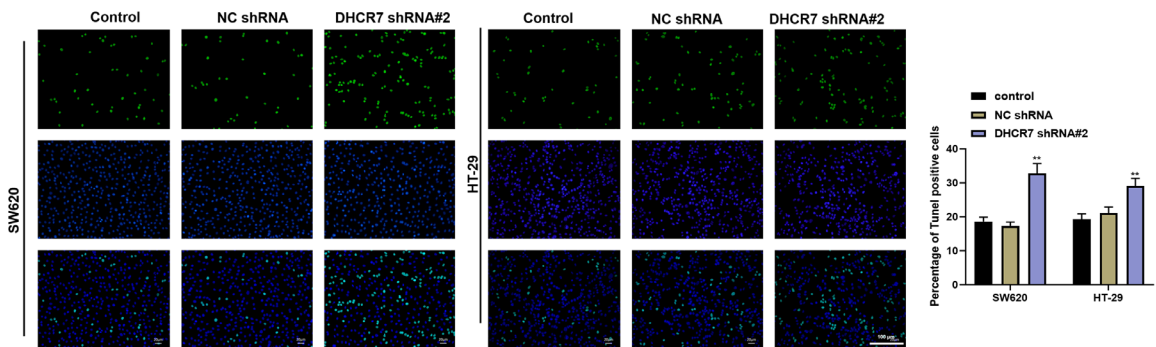


**Figure 10.** Depletion of DHCR7 induced apoptosis in CRC cells. The Terminal deoxynucleotidyl transferase dUTP Nick End Labeling (TUNEL) staining assay was employed to evaluate the apoptosis in SW620 and HT-29 cells following transfection with DHCR7 shRNA #2. Scale bar: 100  $\mu$ m, 100 $\times$ . Data: Mean  $\pm$  Standard Error of the Mean (SEM), n = 3. \*\*P < 0.01, compared to Negative Control (NC) shRNA group.

## Identifying lipid biomarkers in CRC

have shown that, in addition to the well-known role of lipid-related enzymes in providing energy and building blocks for cancer cells, lipid metabolism-related genes can also influence the tumor microenvironment. For example, lipid-associated signaling pathways can modulate immune cell infiltration and function, affecting the immune response against CRC cells [14]. Moreover, abnormal lipid metabolism can lead to the production of bioactive lipid species, which can modulate cell-cell communication and promote tumor cell invasion and metastasis [15]. Despite this, few studies have explored the involvement of lipid metabolism-related genes in regulating CRC.

The unique perspective of this study lies in its comprehensive approach of integrating multiple bioinformatics methods, including WGCNA and PPI network analysis, to systematically screen for lipid metabolism-related genes in CRC. This differs from previous studies that focus on individual genes or pathways. By using WGCNA, we were able to construct gene co-expression networks and identify modules closely related to CRC, offering a global view of gene-gene interactions. Subsequent PPI network analysis and hub gene identification further pinpointed key genes within these modules. Additionally, we not only examined the differential expression of genes but also explored the regulatory networks involving miRNAs and transcription factors, which has not been comprehensively studied in the context of CRC and lipid metabolism. This multi-level analysis may uncover new regulatory mechanisms and potential therapeutic targets in CRC.

This study combined multiple bioinformatics methods to identify hub genes, including WGCNA and PPI, ultimately identifying six hub genes: DHCR7, FABP4, FASN, FAXDC2, PTGIS, and SLC27A6. Based on ROC analysis and rigorous scientific verification, we found that several of these biomolecules, such as DHCR7 and FABP, exhibit extremely high sensitivity and specificity in CRC diagnosis. Therefore, these genes are considered key biomarkers for CRC diagnosis. Notably, DHCR7, a key enzyme in the cholesterol biosynthesis pathway, plays a critical role in regulating the balance between cholesterol synthesis and vitamin D [16]. Recent studies have shown that the DHCR7 expression is closely related to cancer development. For example, Zou *et al.* [17] revealed a significant

correlation between elevated DHCR7 expression and decreased survival rate in cervical cancer patients, as well as a correlation with the infiltration of T cells (especially CD8 T cells). This emphasizes the importance of DHCR7 in cancer research. Li *et al.* [18] illustrated that DHCR7 upregulation in bladder cancer serves as an independent risk factor, correlating with tumor grading and staging, and ultimately poor prognosis. DHCR7 overexpression accelerates G0/G1 phase tumor cell growth, inhibits apoptosis, enhances invasion, migration, and EMT through the PI3K/AKT/mTOR pathway. FABP4, a member of the FABP family, is predominantly found in mature adipocytes and macrophages [19]. It binds reversibly to hydrophobic ligands and regulates transcription, cell signaling, lipid droplet storage, lipid oxidation, and membrane synthesis [20]. Zhang *et al.* [21] showed that FABP4 expression is elevated in CRC tissues and is closely related to the TNM staging in CRC. Gao *et al.* [22] suggested that depletion of FABP4 inhibits CRC progression by regulating cell growth, stemness, glycolysis, and apoptosis. Fatty acid synthase gene (FASN) is highly expressed in human tissues, including the liver, lung, breast, and adipose tissues. Immunohistochemical studies have shown that FASN expression is abnormally high in a variety of human epithelial cancers and precancerous lesions, including breast cancer and CRC, and is associated with the occurrence and development of these cancers [15, 23-26]. In contrast, inhibition of FAS results in the accumulation of malonyl CoA, which inhibits CPT-1, up-regulates ceramide expression, and induces pro-apoptotic genes such as BNIP3, TRAIL, and DAPK2 [27]. Research has shown that FASN is highly expressed in most CRC cases, especially in advanced CRC, and its expression intensity correlates with CRC patient survival rates, with FASN overexpression linked to poorer survival [28]. FAXDC2, a member of the fatty acid hydroxylase family, plays a crucial role in the synthesis and metabolism of fatty acids [29]. Peng *et al.* [30] identified FAXDC2 as an effective inhibitor of hepatocellular carcinoma for the first time, suggesting that it inhibits tumor cell proliferation and invasion through mechanisms related to ERK signaling. PTGIS, a key enzyme in arachidonic acid metabolism, belongs to the cytochrome P450 superfamily (CYP8) [31]. It plays an important role in a wide range of physiological and pathological pro-

## Identifying lipid biomarkers in CRC

cesses, and many studies have recognized PTGIS as an inhibitor of multiple tumor types. At the same time, PTGIS is also a key candidate gene in cardiovascular disease research, linked to conditions such as hypertension, myocardial infarction, stroke and atherosclerosis [32, 33]. Ding *et al.* [34] found that PTGIS expression is relatively low in CRC. SLC27A, a class of transmembrane protein, promotes intracellular long-chain fatty acid uptake. There are six isoforms of the SLC27A family (SLC27A1~6), all involved in fatty acid transport [35]. Zhong *et al.* [36] showed that overexpression of SLC27A6 in nasopharyngeal carcinoma cell lines significantly inhibited cell proliferation and tumorigenesis. In this study, we compared and analyzed the expression of hub genes in CRC patients versus the TCGA normal group. The results showed that genes such as FABP4 and FAXDC2 were downregulated in CRC patients, while DHCR7 and FASN expression levels were elevated. Additionally, we collected 54 pairs of CRC tissues and adjacent non-cancerous tissues and used immunohistochemical staining to verify the expression levels of six hub genes. The verification results confirmed that in CRC tissues, FAXDC2, PTGIS, and SLC27A6 expression levels were decreased, while FASN and DHCR7 expression levels were increased. However, it was noteworthy that the expression trend of FABP4 in CRC tissues did not match the bioinformatics predictions, with its expression level significantly elevated in CRC tissues.

The upregulation of DHCR7 and FASN in CRC tissues is consistent with previous reports in some cancers. However, our study not only confirmed their overexpression in CRC but also demonstrated their potential as diagnostic biomarkers through ROC curve analysis. The high AUC values for DHCR7 and FASN indicate their strong diagnostic performance. For FAXDC2 and PTGIS, our observation of their downregulation in CRC provides new insights. Previous studies on these genes in CRC are limited, and our results suggest that they may play a suppressive role in CRC development. The abnormal expression of FABP4 and SLC27A6, which deviated from bioinformatics predictions, also highlights the complexity of gene regulation in CRC. These findings prompt us to further explore the underlying molecular mechanisms, which may involve different signaling pathways and regulatory networks in CRC.

The inconsistent expression trends of FABP4 and SLC27A6 genes compared to bioinformatics predictions are intriguing. For FABP4, one possible reason is the complex regulation of this gene in different cellular contexts. Although bioinformatics analyses are based on large-scale datasets, they may not fully capture the tissue-specific or microenvironment-dependent regulatory mechanisms. In CRC tissues, local factors, such as specific cytokines, growth factors, or epigenetic modifications, may override the general trends predicted by bioinformatics. Another possibility is that the databases used for bioinformatics analysis may have limitations in representing the full spectrum of CRC patient heterogeneity. Regarding SLC27A6, the lack of significant difference in expression between CRC tissues and adjacent non-cancerous tissues in our clinical validation may be due to small sample size. A larger cohort might reveal a clearer and more statistically robust expression pattern. Additionally, SLC27A6 may have a more complex regulatory mechanism in CRC, which could involve post-translational modifications or interactions with other proteins that were not accounted for in our bioinformatics analysis. Future studies with larger sample sizes and more in-depth molecular analysis are needed to fully understand the reasons for these discrepancies.

After a series of bioinformatic analyses and clinical validation, this study concluded that the lipid metabolism-related genes FAXDC2, PTGIS, FABP4, and SLC27A6 are down-regulated, while FASN and DHCR7 are up-regulated in the TCGA-CRC and GEO-CRC databases. Immunohistochemistry-based validation in clinical CRC tissues confirmed that the expression trends of FAXDC2, PTGIS, SLC27A6, FASN, and DHCR7 were consistent with bioinformatics predictions (**Figure 11**). However, the expression of FABP4 in CRC tissues differed from the bioinformatics prediction, which may be due to the limited data available in the database. To gain a deeper understanding of the specific mechanisms underlying FABP4's differential expression, we plan to expand the dataset and conduct more in-depth analysis. Overall, this study successfully identified six characteristic genes closely related to lipid metabolism. These findings not only enhance our understanding of CRC pathogenesis but also indicate that these biomarkers may provide new diag-

## Identifying lipid biomarkers in CRC

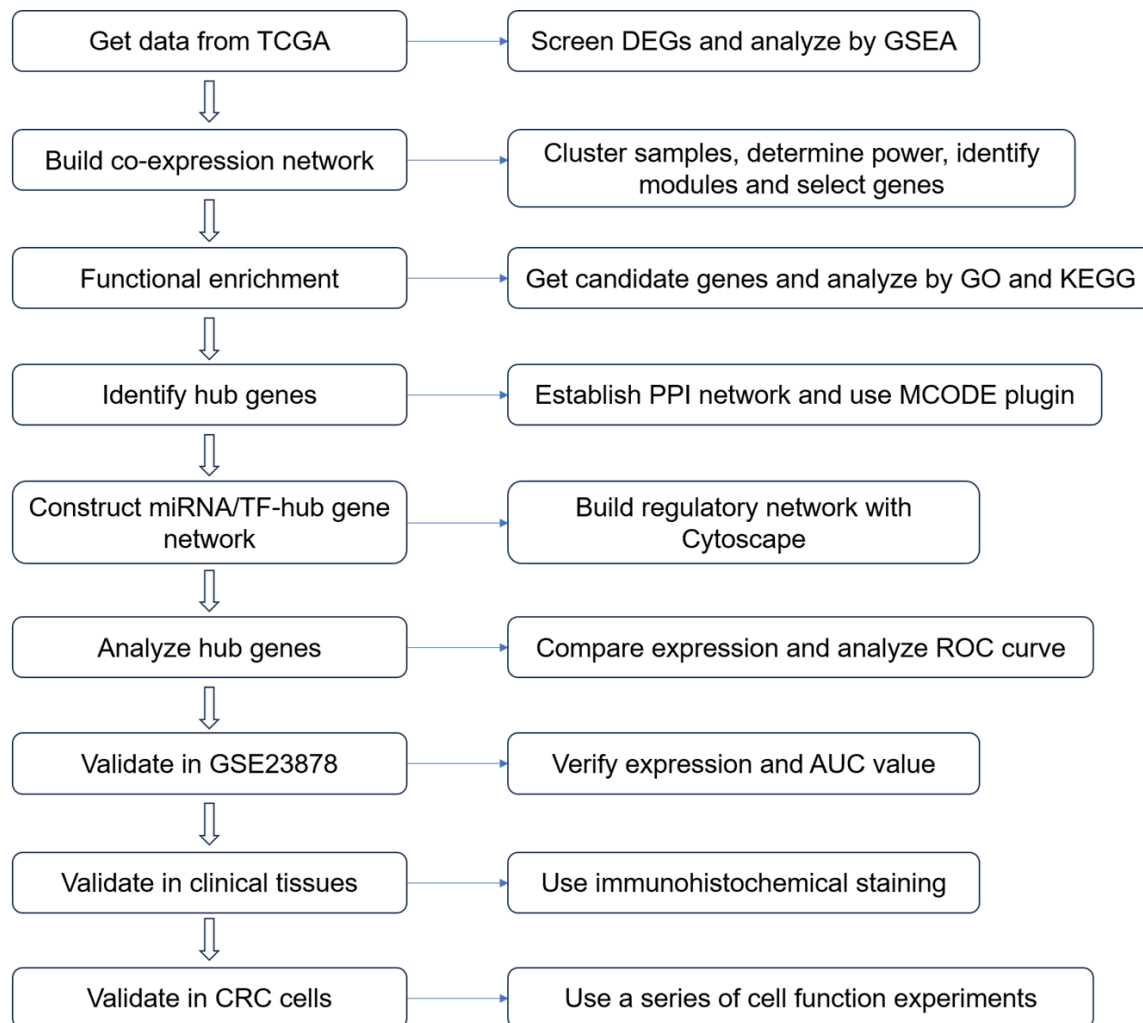


**Figure 11.** Experimental procedure. This study began with data extraction from The Cancer Genome Atlas (TCGA), followed by the identification of Differentially Expressed Genes (DEGs) and Gene Set Enrichment Analysis (GSEA). A gene co-expression network was then constructed to detect modules and perform functional enrichment analysis, identifying key candidate genes. Hub genes were pinpointed through protein-protein interaction analysis and the Molecular Complex Detection (MCODE) plugin. This study constructed a detailed miRNA (microRNA)/TF (transcription factor) central gene regulatory network aimed at revealing the complex interactions between these molecules. To further explore the potential of central genes in practical applications, this study further adopted Receiver Operating Characteristic (ROC) curve analysis to evaluate the diagnostic value of these hub genes, and carefully examined their expression levels under different conditions. Validation of these genes was conducted using the GSE23878 dataset and immunohistochemical staining on clinical tissues.

nostic and treatment strategies for CRC patients in the future, ultimately improving the prognosis and quality of life of CRC patients.

### Acknowledgements

This research is supported by National Natural Science Foundation of China (No. 82272909).

### Disclosure of conflict of interest

None.

**Address correspondence to:** Baokun Li, Second Departments Surgery, The Fourth Hospital of Hebei Medical University, No. 12 Jiankang Road, Shijiazhuang 050000, Hebei, China. E-mail: libaokun@hebmh.edu.cn

### References

- [1] Sung H, Ferlay J, Siegel RL, Laversanne M, Soerjomataram I, Jemal A and Bray F. Global cancer statistics 2020: GLOBOCAN estimates of incidence and mortality worldwide for 36

## Identifying lipid biomarkers in CRC

- cancers in 185 countries. *CA Cancer J Clin* 2021; 71: 209-249.
- [2] Biller LH and Schrag D. Diagnosis and treatment of metastatic colorectal cancer: a review. *JAMA* 2021; 325: 669-685.
- [3] Sakamaki JI and Mizushima N. Cell biology of protein-lipid conjugation. *Cell Struct Funct* 2023; 48: 99-112.
- [4] Snaebjornsson MT, Janaki-Raman S and Schulze A. Greasing the Wheels of the cancer machine: the role of lipid metabolism in cancer. *Cell Metab* 2020; 31: 62-76.
- [5] Krauß D, Fari O and Sibilia M. Lipid metabolism interplay in CRC-an update. *Metabolites* 2022; 12: 213.
- [6] Yang Z, Xiao H, Jin H, Koo PT, Tsang DJ and Yang CS. Synergistic actions of atorvastatin with gamma-tocotrienol and celecoxib against human colon cancer HT29 and HCT116 cells. *Int J Cancer* 2010; 126: 852-863.
- [7] Dai W, Xiang W, Han L, Yuan Z, Wang R, Ma Y, Yang Y, Cai S, Xu Y, Mo S, Li Q and Cai G. PT-PRO represses colorectal cancer tumorigenesis and progression by reprogramming fatty acid metabolism. *Cancer Commun (Lond)* 2022; 42: 848-867.
- [8] Yang Y, Luo D, Shao Y, Shan Z, Liu Q, Weng J, He W, Zhang R, Li Q, Wang Z and Li X. circCAPRIN1 interacts with STAT2 to promote tumor progression and lipid synthesis via upregulating ACC1 expression in colorectal cancer. *Cancer Commun (Lond)* 2023; 43: 100-122.
- [9] Han L, Dai W, Luo W, Ye L, Fang H, Mo S, Li Q, Xu Y, Wang R and Cai G. Enhanced de novo lipid synthesis mediated by FASN induces chemoresistance in colorectal cancer. *Cancers (Basel)* 2023; 15: 562.
- [10] Piccinin E, Cariello M and Moschetta A. Lipid metabolism in colon cancer: role of Liver X receptor (LXR) and stearoyl-CoA desaturase 1 (SCD1). *Mol Aspects Med* 2021; 78: 100933.
- [11] Bian X, Liu R, Meng Y, Xing D, Xu D and Lu Z. Lipid metabolism and cancer. *J Exp Med* 2021; 218: e20201606.
- [12] Fernández LP, Gómez de Cedrón M and Ramírez de Molina A. Alterations of lipid metabolism in cancer: implications in prognosis and treatment. *Front Oncol* 2020; 10: 577420.
- [13] Schiliro C and Firestein BL. Mechanisms of metabolic reprogramming in cancer cells supporting enhanced growth and proliferation. *Cells* 2021; 10: 1056.
- [14] Nenkov M, Ma Y, Gaßler N and Chen Y. Metabolic reprogramming of colorectal cancer cells and the microenvironment: implication for therapy. *Int J Mol Sci* 2021; 22: 6262.
- [15] Ecker J, Benedetti E, Kindt ASD, Höring M, Perl M, Machmüller AC, Sichler A, Plagge J, Wang Y, Zeissig S, Shevchenko A, Burkhardt R, Krum-siek J, Liebisch G and Janssen KP. The colorectal cancer lipidome: identification of a robust tumor-specific lipid species signature. *Gastroenterology* 2021; 161: 910-923, e919.
- [16] Prabhu AV, Luu W, Li D, Sharpe LJ and Brown AJ. DHCR7: a vital enzyme switch between cholesterol and vitamin D production. *Prog Lipid Res* 2016; 64: 138-151.
- [17] Zou J, Liu S, Long J and Yan B. High DHCR7 expression predicts poor prognosis for cervical cancer. *Comput Math Methods Med* 2022; 2022: 8383885.
- [18] Li Y, Zhou Y, Huang M, Wang Z, Liu D, Liu J, Fu X, Yang S, Shan S, Yang L, Guo Y, Ren P, Chen P, Zeng G, Guo Y, Wang X, DiSanto ME and Zhang X. DHCR7 promotes tumorigenesis via activating PI3K/AKT/mTOR signalling pathway in bladder cancer. *Cell Signal* 2023; 102: 110553.
- [19] Guo D, Lin C, Lu Y, Guan H, Qi W, Zhang H, Shao Y, Zeng C, Zhang R, Zhang H, Bai X and Cai D. FABP4 secreted by M1-polarized macrophages promotes synovitis and angiogenesis to exacerbate rheumatoid arthritis. *Bone Res* 2022; 10: 45.
- [20] Liu S, Wu D, Fan Z, Yang J, Li Y, Meng Y, Gao C and Zhan H. FABP4 in obesity-associated carcinogenesis: novel insights into mechanisms and therapeutic implications. *Front Mol Biosci* 2022; 9: 973955.
- [21] Zhang Y, Zhang W, Xia M, Xie Z, An F, Zhan Q, Tian W and Zhu T. High expression of FABP4 in colorectal cancer and its clinical significance. *J Zhejiang Univ Sci B* 2021; 22: 136-145.
- [22] Gao Y, Wang Y, Wang X, Ma J, Wei M, Li N and Zhao Z. FABP4 regulates cell proliferation, stemness, apoptosis, and glycolysis in colorectal cancer via modulating ROS/ERK/mTOR pathway. *Discov Med* 2023; 35: 361-371.
- [23] Chaturvedi S, Biswas M, Sadhukhan S and Sonawane A. Role of EGFR and FASN in breast cancer progression. *J Cell Commun Signal* 2023; 17: 1249-1282.
- [24] Bastos DC, Ribeiro CF, Ahearn T, Nascimento J, Pakula H, Clohessy J, Mucci L, Roberts T, Zanata SM, Zadra G and Loda M. Genetic ablation of FASN attenuates the invasive potential of prostate cancer driven by Pten loss. *J Pathol* 2021; 253: 292-303.
- [25] Chen R, Hao X, Chen J, Zhang C, Fan H, Lian F, Chen X, Wang C and Xia Y. Integrated multi-omics analyses reveal Jorunnamycin A as a novel suppressor for muscle-invasive bladder cancer by targeting FASN and TOP1. *J Transl Med* 2023; 21: 549.
- [26] Jiang L, Wang H, Li J, Fang X, Pan H, Yuan X and Zhang P. Up-regulated FASN expression pro-

## Identifying lipid biomarkers in CRC

- motes transcoelomic metastasis of ovarian cancer cell through epithelial-mesenchymal transition. *Int J Mol Sci* 2014; 15: 11539-11554.
- [27] Schroeder B, Vander Steen T, Espinoza I, Venkatapoorna CMK, Hu Z, Silva FM, Regan K, Cuyàs E, Meng XW, Verdura S, Arbusà A, Schneider PA, Flatten KS, Kemble G, Montero J, Kaufmann SH, Menendez JA and Lupu R. Fatty acid synthase (FASN) regulates the mitochondrial priming of cancer cells. *Cell Death Dis* 2021; 12: 977.
- [28] Wei W, Qin B, Wen W, Zhang B, Luo H, Wang Y, Xu H, Xie X, Liu S, Jiang X, Wang M, Tang Q, Zhang J, Yang R, Fan Z, Lyu H, Lin J, Li K and Lee MH. FBXW7 $\beta$  loss-of-function enhances FASN-mediated lipogenesis and promotes colorectal cancer growth. *Signal Transduct Target Ther* 2023; 8: 187.
- [29] Jin Q, Ren Y, Wang M, Suraneni PK, Li D, Crispino JD, Fan J and Huang Z. Novel function of FAXDC2 in megakaryopoiesis. *Blood Cancer J* 2016; 6: e478.
- [30] Peng Z, Xu S, Zhang Q, Yang X, Yuan W, Wang Y, Li Y, Zhu P, Wu X, Jiang Z, Li F and Fan X. FAXDC2 inhibits the proliferation and invasion of human liver cancer HepG2 cells. *Exp Ther Med* 2023; 27: 27.
- [31] Peng H, Weng L, Lei S, Hou S, Yang S, Li M and Zhao D. Hypoxia-hindered methylation of PTGIS in endometrial stromal cells accelerates endometriosis progression by inducing CD16(-) NK-cell differentiation. *Exp Mol Med* 2022; 54: 890-905.
- [32] Wang XJ, Xu XQ, Sun K, Liu KQ, Li SQ, Jiang X, Zhao QH, Wang L, Peng FH, Ye J, Wu Y, Jiang R, Zhang J, Huang W, Wei WB, Yan Y, Li JH, Liu QQ, Li S, Wang Y, Zhang SY, Zhang X and Jing ZC. Association of rare PTGIS variants with susceptibility and pulmonary vascular response in patients with idiopathic pulmonary arterial hypertension. *JAMA Cardiol* 2020; 5: 677-684.
- [33] Nakayama T. Genetic polymorphisms of prostacyclin synthase gene and cardiovascular disease. *Int Angiol* 2010; 29 Suppl: 33-42.
- [34] Ding H, Wang KY, Chen SY, Guo KW and Qiu WH. Validating the role of PTGIS gene in colorectal cancer by bioinformatics analysis and in vitro experiments. *Sci Rep* 2023; 13: 16496.
- [35] Gallardo D, Amills M, Quintanilla R and Pena RN. Mapping and tissue mRNA expression analysis of the pig solute carrier 27A (SLC27A) multigene family. *Gene* 2013; 515: 220-223.
- [36] Zhong X, Yang Y, Li B, Liang P, Huang Y, Zheng Q, Wang Y, Xiao X, Mo Y, Zhang Z, Zhou X, Huang G and Zhao W. Downregulation of SLC27A6 by DNA hypermethylation promotes proliferation but suppresses metastasis of nasopharyngeal carcinoma through modulating lipid metabolism. *Front Oncol* 2022; 11: 780410.